Supporting Information

Electrocatalytic Reaction of N_2 and Nitrogen Incorporation Process on Dopant-free Defect Graphene

Yanqiu Du [a], Cheng Jiang [a], Wei Xia [a], Li Song [a], Peng Li [a], Bin Gao [a], Chao Wu [a], Lei Sheng [a], Jinhua Ye [b], Tao Wang [a] and Jianping He [a]**

[a]College of Materials Science and Technology, Jiangsu Key Laboratory of Electrochemical Energy Storage Technologies, Nanjing University of Aeronautics and Astronautics, 29 Yudao Street, Nanjing, 210016 (P. R. China)

[b]International Center for Materials Nanoarchitectonics (WPI-MANA), National Institute for Materials Science (NIMS), 1-1 Namiki, Tsukuba, Ibaraki 305-0044 (Japan)

***Corresponding Author**

Prof. Tao Wang, Tel: +86 25 52112900; Fax: +86 25 52112626,
E-mail: wangtao0729@nuaa.edu.cn;
Prof. Jianping He, Tel: +86 25 52112900; Fax: +86 25 52112626,
E-mail: jianph@nuaa.edu.cn;

Table of Contents

I. Supplementary Methods

1. Synthesis of DG

Firstly, graphite oxide was prepared from flaky graphite by a modified Hummers method. The frozen-dried graphite oxide and molten salts, which consists of LiCl/KCl (mass ratio=45:55) were mixed by grinding method for several minutes. The mixture was annealed in N_2 at 400 °C and 800 °C for 2 h, respectively, with a heating rate of 2 °C /min. To completely remove the molten salts, the mixture was soaked in deionized water and stirred for 24 h. Then, the product was collected by centrifugation and dried under a vacuum at 80 °C. The as-prepared samples annealed at different temperature were labeled as DG-X, where X represented the temperature. For comparison, the frozen-dried GO that directly annealed in the same way without molten salts was denoted as pristine graphene (PG).

2. Characterization

The structure information was obtained by X-ray diffraction (XRD) on Rigaku D/max-2000 diffractometer with Cu Kα radiation. The morphological information was collected on a Hitachi Co. S4800 field emission scanning electron microscopy and transmission electron microscopy (Tecnai G2 F30 S-TWIN). The aberration-corrected high-angle annular dark-field scanning transmission electron microscopy image were taken on a FEI Themis TEM operating at 200 Kv. The X-ray photoelectron spectroscopy (XPS) was obtained on Thermo ESCALAB 250XI. The FT-IR spectras were recorded on a Nicolet FT-IR 6700 spectrophotometer. The post-electrolysis electrodes were grinded with KBr to collect the information of variation. The specific surface area of the samples was calculated by the Brunauer–Emmett–Teller (BET) method and the pore size distributions were determined by the Barrett–Joyner–Halenda (BJH) method on a Micromeritics ASAP 2010 instrument.

3. Electrochemical measurements

All electrochemical measurements were conducted in a typical three-electrode system, in which platinum (Pt) foil and a saturated Ag/AgCl electrode were used as counter and reference electrode, respectively. For the fabrication of the working electrode, 2.0 mg of the sample was dispersed in 0.95 mL isopropanol and 0.05 mL Nafion solution (5.0

wt%), followed by 30min sonication to prepare a homogeneous ink. The 1 mL ink was sprayed onto the 2×2 cm^2 carbon paper, which was ultrasonically washed by ethanol and acetone in advance.

The NRR measurements were carried out in 0.01 M H_2SO_4 with continuous N_2 flow. The anode chamber and cathode chamber were separated by Nafion 211 membrane, which was boiled in 3% H_2O_2, 0.5 M H_2SO_4 for 1 h, respectively. The chronoamperometry tests were performed at different potentials (-0.3 V, -0.4 V, -0.5 V and -0.6 V vs. RHE).

4. Quantification test

The concentration of NH_4^+, produced during the chronoamperometry tests, was measured by Nessler reagent and indophenol blue method.[1] To eliminate environmental contamination, the electrolytes were stored at low temperature. The time stained with indicator was carefully controlled, thus to get convincing result. For the Nessler reagent method, 3 mL electrolyte removed from cathode chamber after the chronoamperometry test was mixed with 150 uL Nessler reagent, whose absorbance was recorded at 420 nm after 10 min. Each sample was retested for three times. A series of reference solutions with NH_4Cl concentrations (0.1 μg mL^{-1}, 0.2 μg mL^{-1}, 0.4 μg mL^{-1}, 0.8 μg mL^{-1}, 1.6 μg mL^{-1}) in 0.01 M H_2SO_4 was measured in the same way to obtain the standard curve. For indophenol blue method, 4 mL electrolyte after test was mixed with 50 μL oxidizing solution containing NaClO (ρCl = 4–4.9) and NaOH (0.75 M), 500 μL coloring solution containing 0.4 M $C_7H_6O_3$ and 0.32 M NaOH, and 50 μL catalyst solution (1 wt% $Na_2[Fe(CN)_5NO]$). After 2 h, the absorption spectrum was recorded at 690 nm using an ultraviolet-visible (UV-vis) spectrophotometer. Each sample was retested for three times. In the same way, a series of reference solutions with NH_4Cl concentrations (0.1 μg mL^{-1}, 0.2 μg mL^{-1}, 0.4 μg mL^{-1}, 0.8 μg mL^{-1}, 1.6 μg mL^{-1}) in 0.01 M H_2SO_4 was measured to obtain the standard curve. The Faradaic efficiency, the consumed charge toward NH_3 with respect to the total charge, was calculated on the following equation:

$$FE = 3F \times c \times V / (17 \times Q)$$

The NH_3 generation rate was determined using the following equation:

Yield rate = (c × V) / (t × S)

Where t is time (h) for NRR and S is the catalyst loading area, F is the Faraday constant (96485.3 C mol^{-1}), c is the measured NH_3 concentration (μg mL^{-1}), V is the total volume of electrolyte (mL).

The N_2H_4 in post-NRR electrolyte was measured by Watt and Chrisps' method:[2] 4g p-$C_9H_{11}NO$ was dissolved in 20 mL concentrated hydrochloric acid and 200 mL ethanol solution. 5 mL of the above color reagent mixed with 5 mL electrolyte, whose absorption spectrum was recorded for incubating 15 min. The standard curve was obtained by recording absorption spectrum of reference solutions with N_2H_4 concentrations (0.1 μg mL^{-1}, 0.2 μg mL^{-1}, 0.4 μg mL^{-1}, 0.6 μg mL^{-1}, 0.8 μg mL^{-1},1.0 μg mL^{-1}).

5. Simulation methods

In this work, the density functional theory (DFT) calculation was performed using the Dmol^3 code.[3] The exchange-correlation interaction was treated by the generalized gradient approximation (GGA) with PBE functional.[4] A double numerical quality basis set with d-type polarization function (DNP) [5] was utilized for all the geometric optimizations, total energy calculations. The core electrons were modeled using effective core pseudopotentials (ECP) by Dolg[6] and Bergner[7]. All calculations were spinning unrestricted. The positions of all the atoms were fully relaxed until the following convergence criterion are met respectively: 0.002 Ha/Å for force, 10^{-5} Ha for total energy and 0.005 Å for displacement. The real space cutoff radius was 4.1 Å. The self-consistent field computations criterion was chosen to be 10^{-6} Ha.

The adsorption energy (E_{ad}) is defined as

$E_{ad}=E_{Surf+N2} - E_{N2} - E_{Surf}$

Where $E_{Surf+N2}$ is the total energy of PG and DG adsorbed with N_2, E_{N2} is the total energy of N_2, and E_{surf} is the total energy of PG and DG.

II. Supplementary Figures

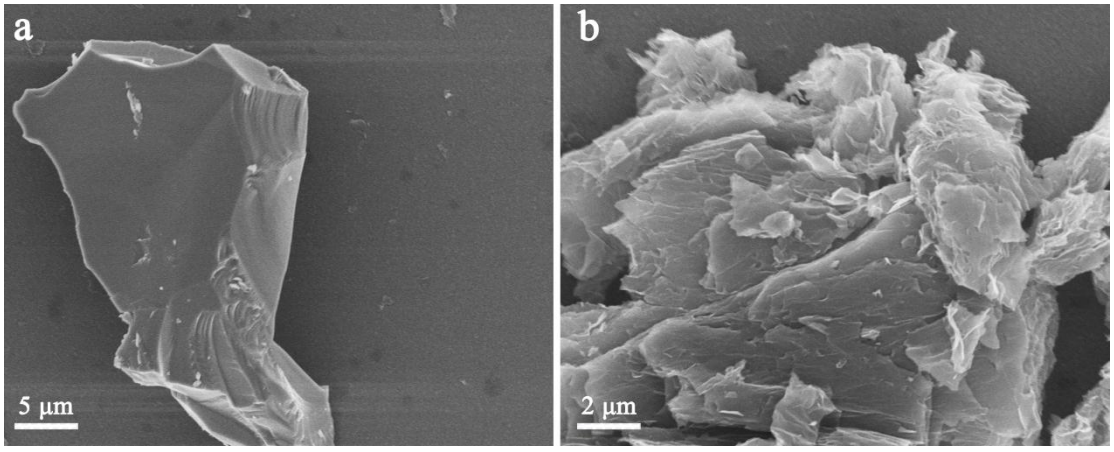

Figure S1 SEM images of bulk oxidized graphite

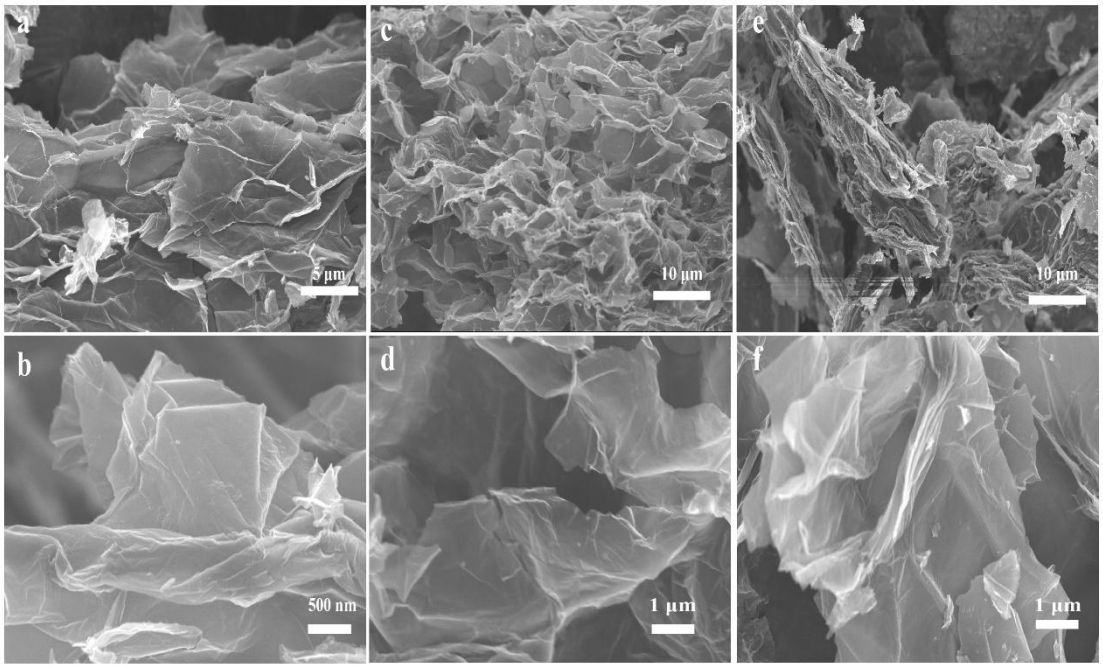

Figure S2 SEM images of defect graphene at different temperature, (a, b) DG-700, (c, d) DG-800, (e, f) DG-900

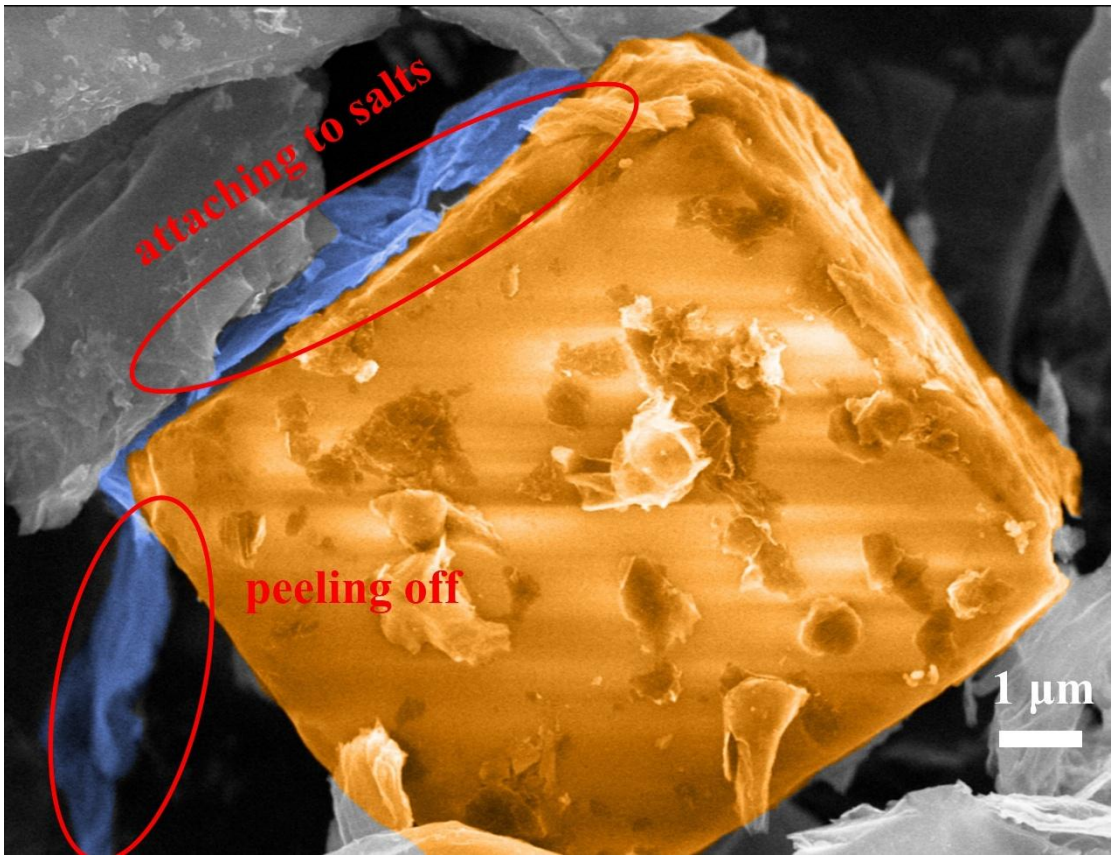

Figure S3 SEM image of graphene @ LiCl /KCl.

As shown in Figure S3, the bulk oxidized graphite was exfoliated in a LiCl/KCl melt, during which the lamellar structure was intercalated with LiCl. Afterwards, the graphene was attached to the cube and peeled off. To totally remove LiCl/KCl, it is performed by washing with water and 2M HCl for 6h.

`

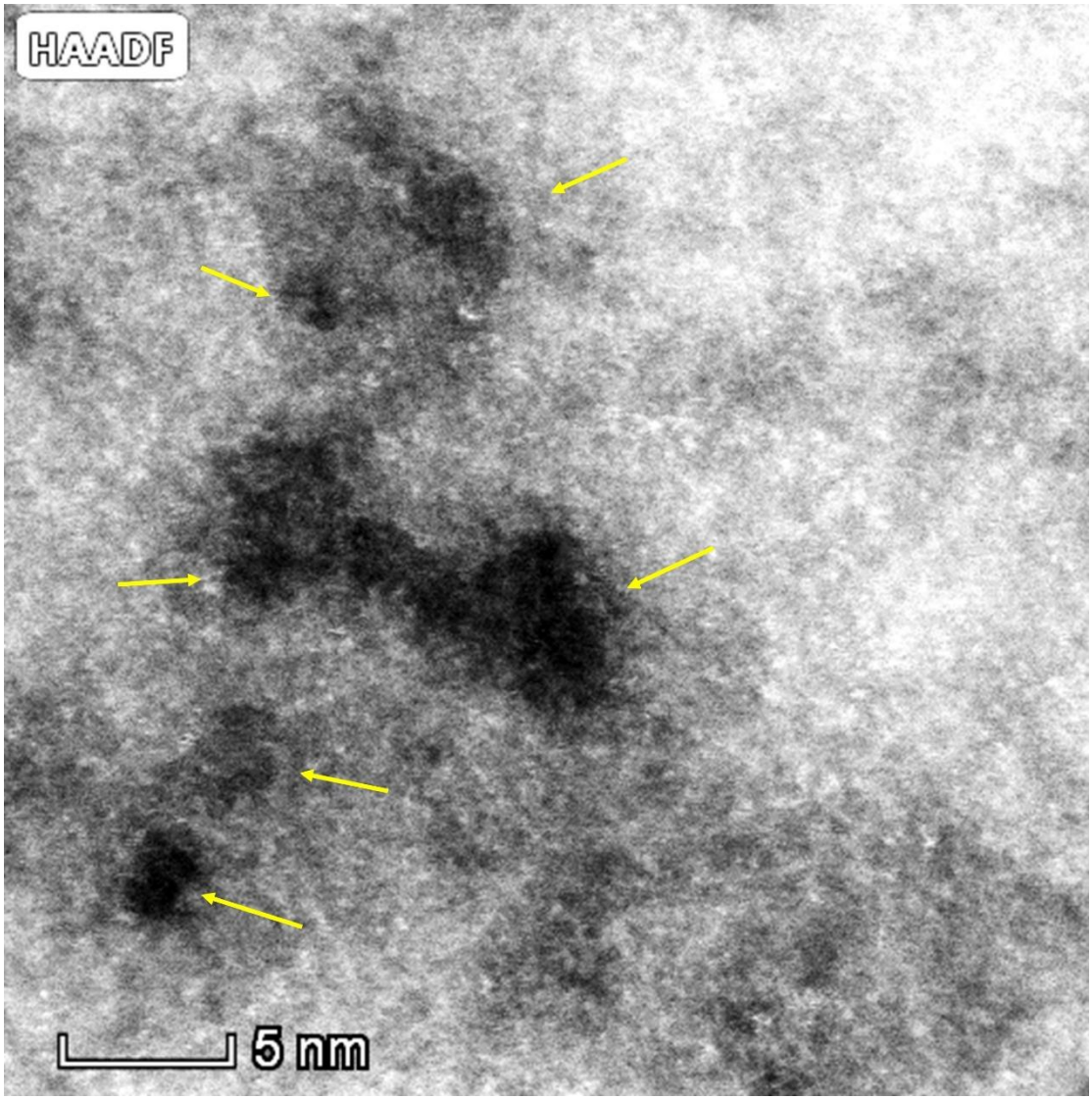

Figure S4 Aberration-corrected high-angle annular dark-field scanning transmission electron microscopy image of DG-800

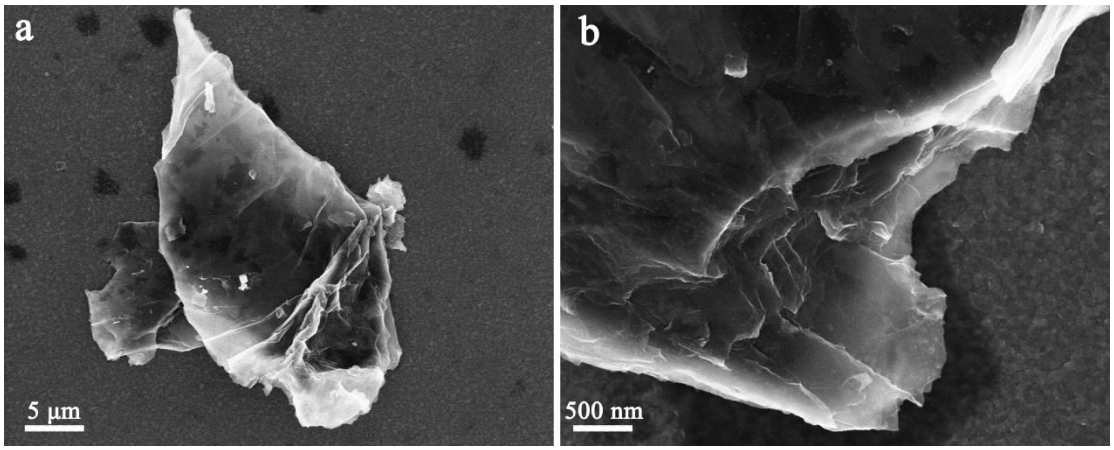

Figure S5 (a, b) SEM images of PG, which is synthesized by directly annealing bulk oxidized graphite.

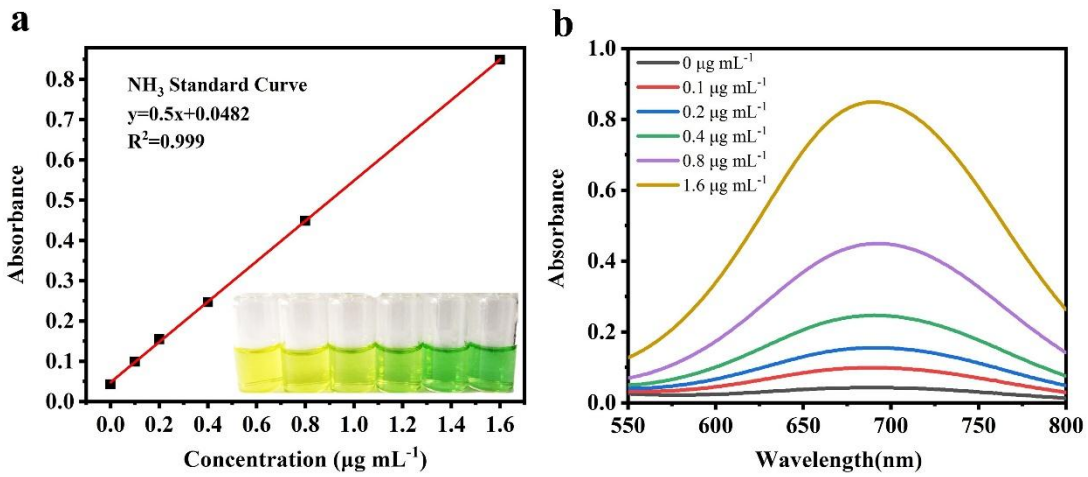

Figure S6 Indophenol blue method using ammonium chloride solutions of known concentration as standards. (a) Calibration curve used for calculation of NH_4^+ concentrations. The inset in (a) shows the chromogenic reaction of the indicator with NH_4^+ (b) UV–vis absorption spectra of standard solution with indophenol indicator after incubated for 2 h at room temperature.

The absorbance at 690 nm was measured and the fitting curve shows good linear relation of absorbance with NH_4^+ ion concentration ($y = 0.5x + 0.0482$, $R^2=0.999$)

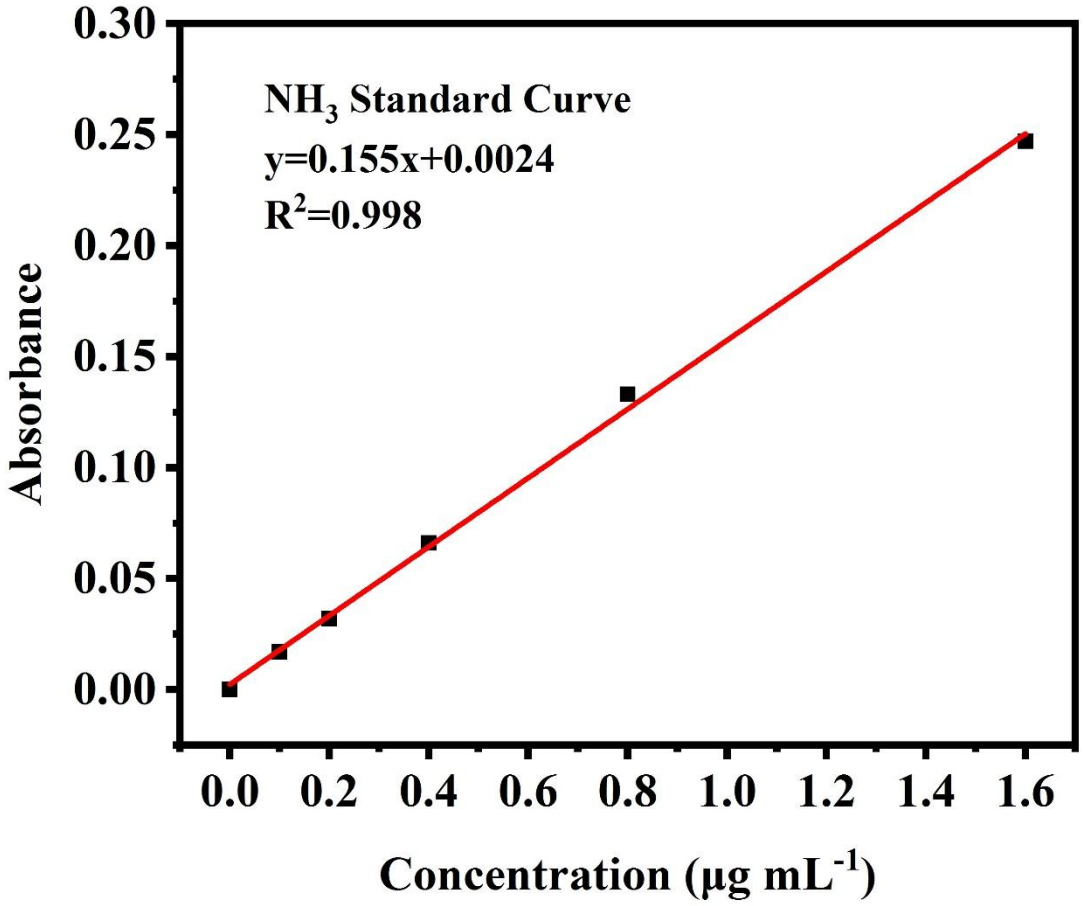

Figure S7 Calibration curve of the Nessler method using ammonium chloride solutions of known concentration as standards.

The absorbance at 420 nm was measured and the fitting curve shows good linear relation of absorbance with NH_4^+ concentration (y = 0.155x +0.0024, R^2=0.998)

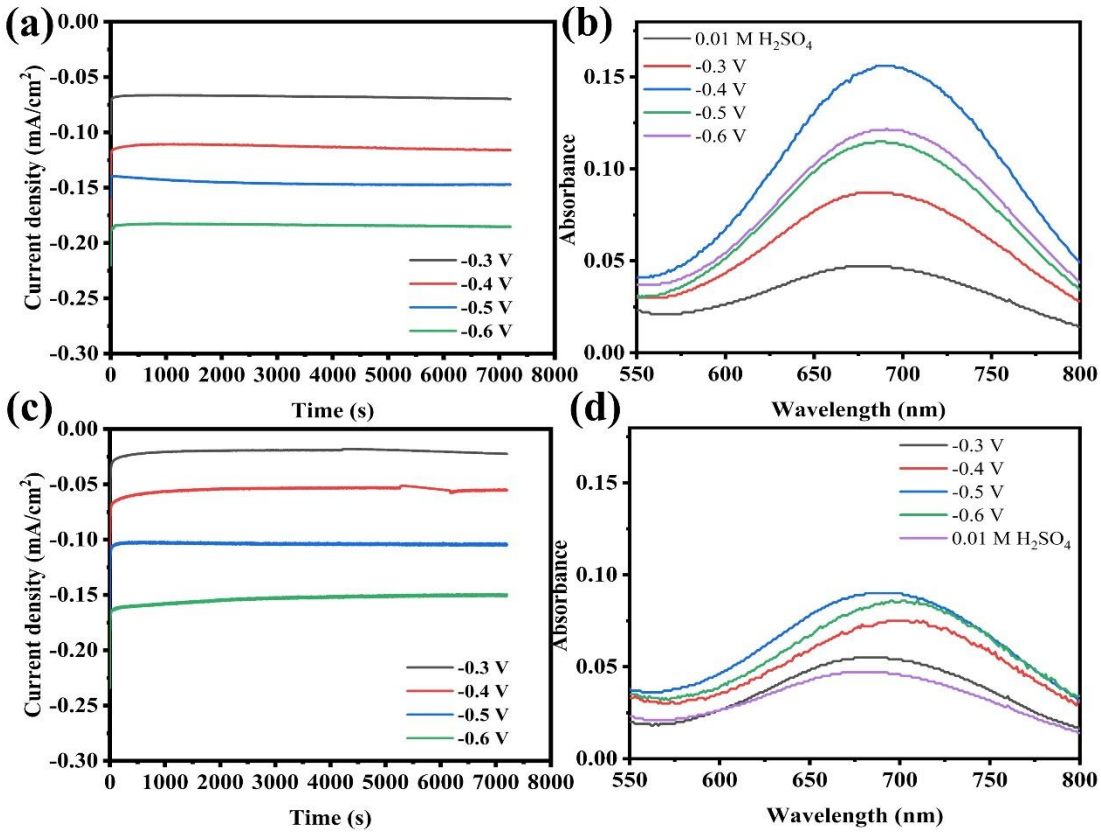

Figure S8 (a) I-t curves of DG-800 at various potentials; (b) Corresponding UV-vis absorption spectra of the electrolyte stained with indicator for NH_3 by using DG-800 as catalyst; (c) I-t curves of PG at various potentials; (d) Corresponding UV-vis absorption spectra of the electrolyte stained with indicator for NH_3 by using PG as catalyst

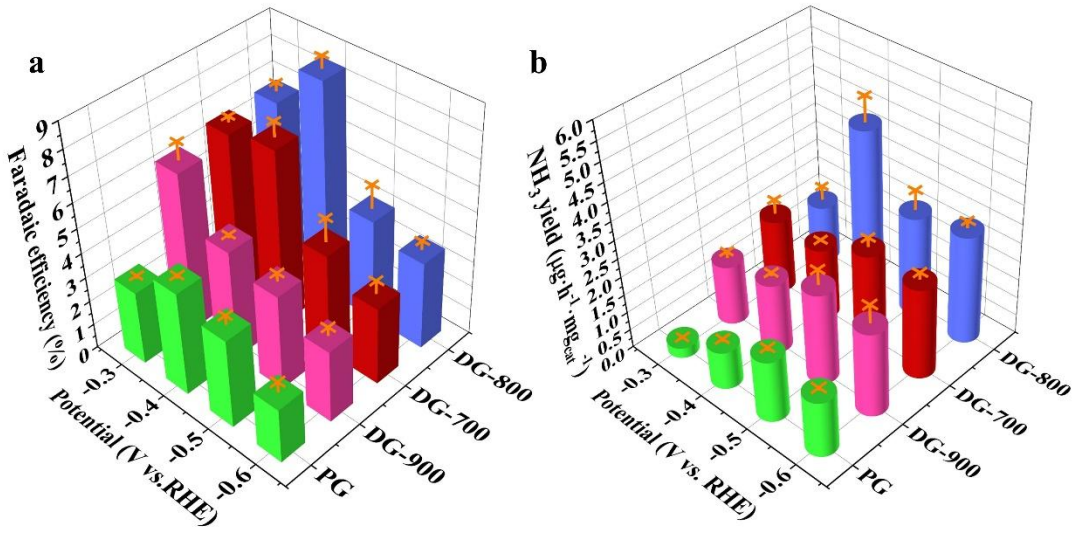

Figure S9 (a) Faradaic efficiency of PG and DG synthesized in different temperature. (b) NH_3 yield rate of PG and DG synthesized in different temperature.

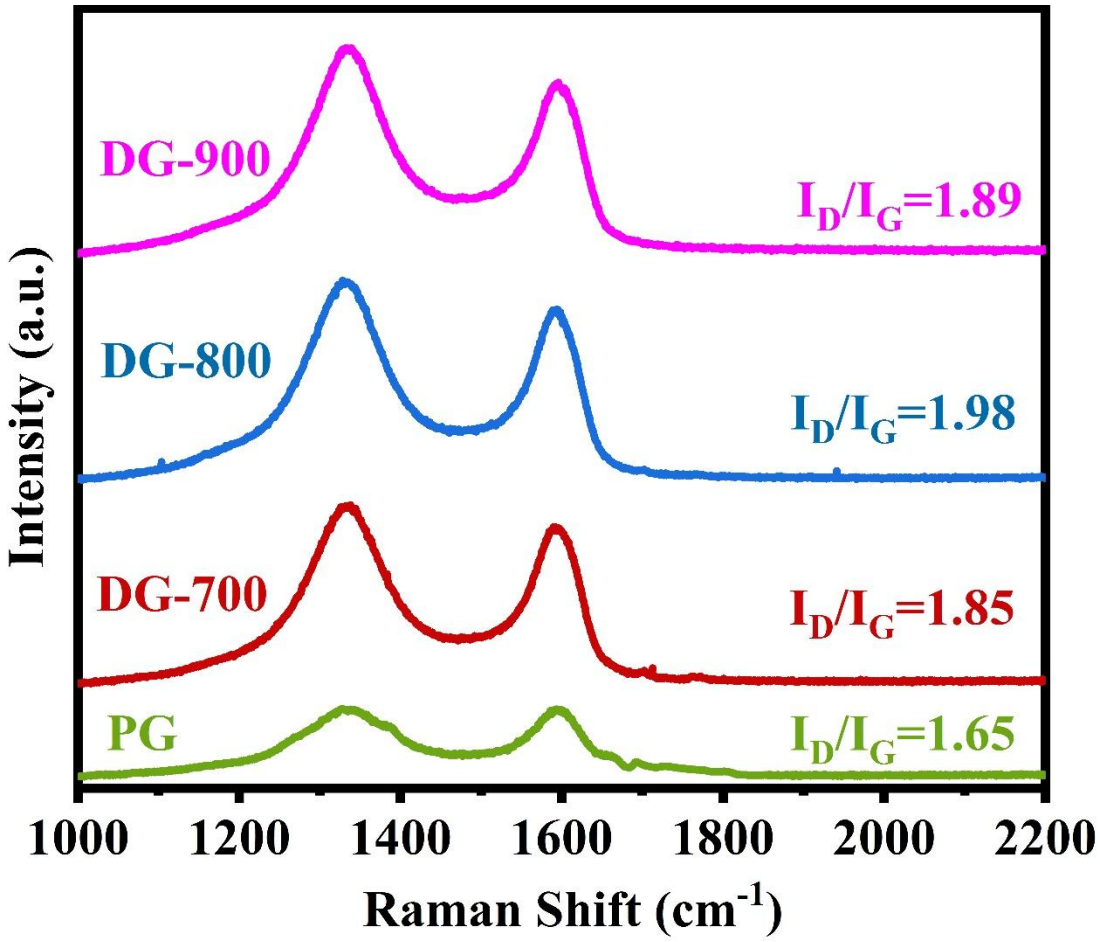

Figure S10 Raman spectra of PG, DG-700, DG-800 and DG-900.

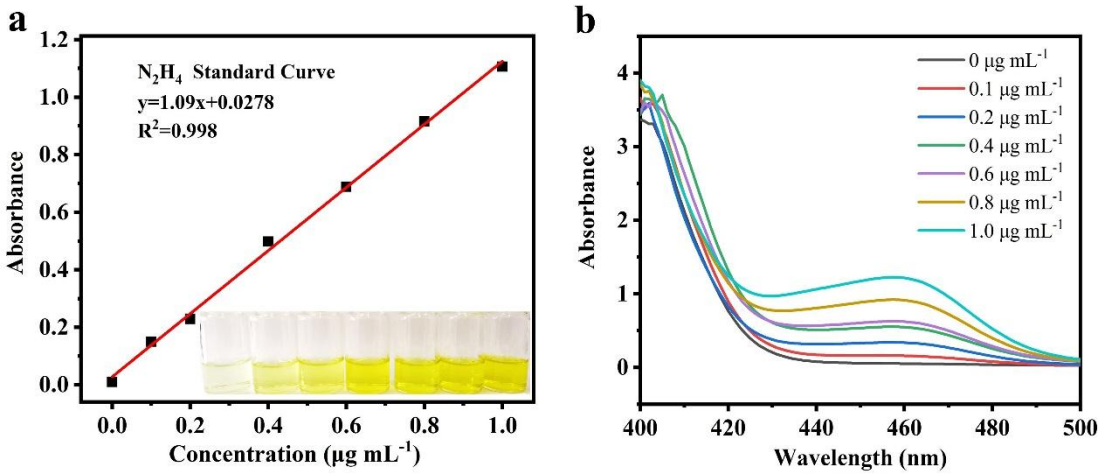

Figure S11 Watt and Chrisp method using $N_2H_4 \cdot H_2O$ of known concentration as standards. (a) Calibration curve used for calculation of N_2H_4 concentrations. The inset in (a) shows the chromogenic reaction of the indicator with NH_4^+ (b) UV–vis absorption spectra of various $N_2H_4 \cdot H_2O$ concentrations after incubation for 15 min at room temperature.

The absorbance at 460 nm was measured and the fitting curve shows good linear relation of absorbance with $N_2H_4 \cdot H_2O$ concentration (y = 1.09x +0.0278, R^2=0.998)

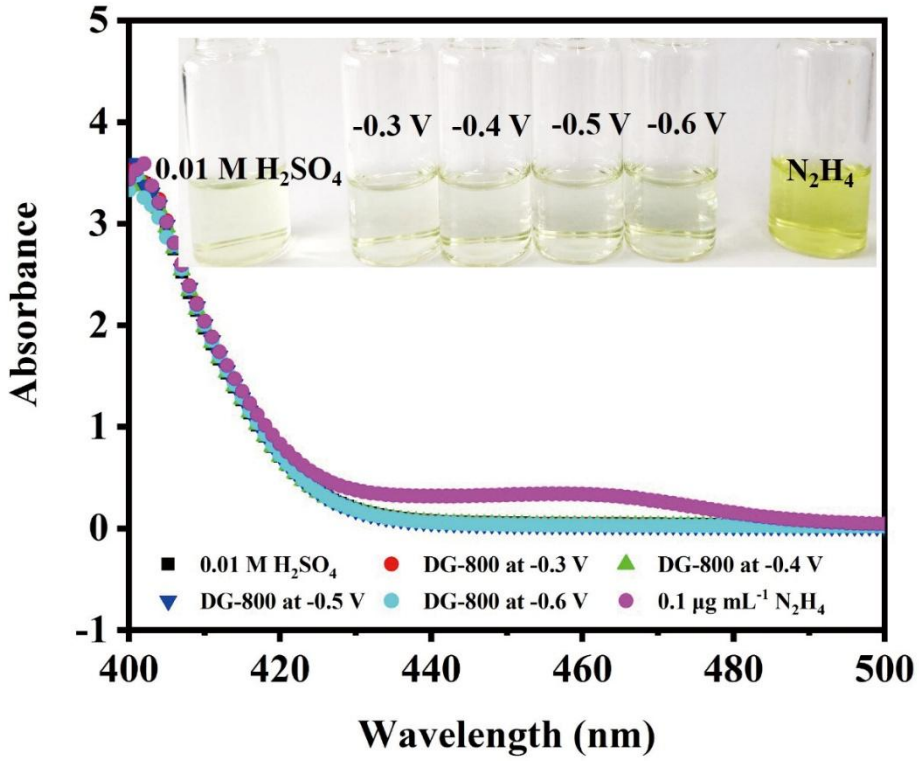

Figure S12 Watt and Chrisp method to detect the presence of N_2H_4 (a) UV–vis absorption spectra of electrolyte stained with indicator for N_2H_4•H_2O, the inset photograph of chromogenic reaction with indicator.

For comparison, N_2H_4•H_2O was evaluated in blank electrolyte and the electrolyte after NRR. No obvious difference can be seen in blank electrolyte (0.01 M H_2SO_4) and electrolyte after test, using DG-800 as electrocatalyst. So, it is reasonable to believe that no by-product was generated in Chronoamperometry tests at different potential.

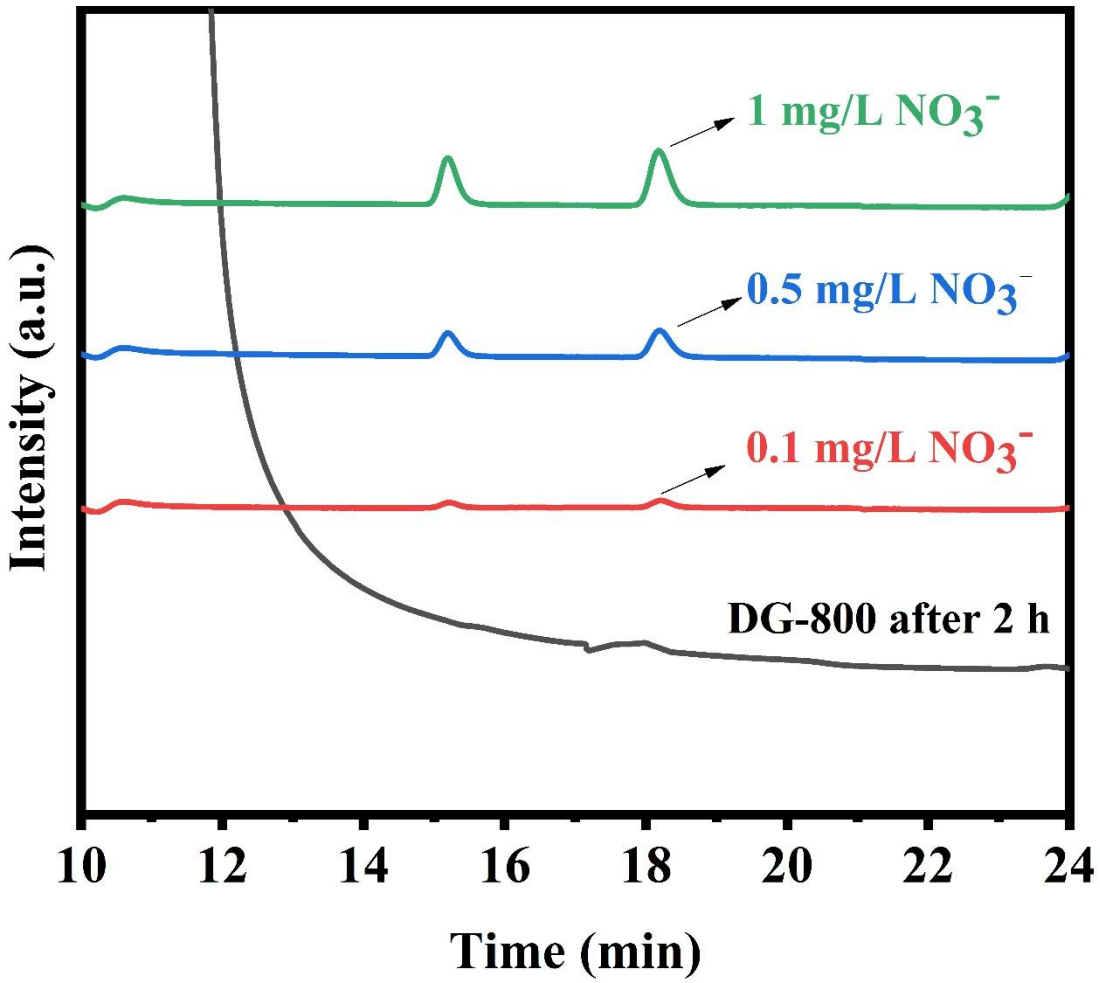

Figure S13 The IC spectra of electrolytes of DG-800 after 2h and NO_3^- at different concentrations

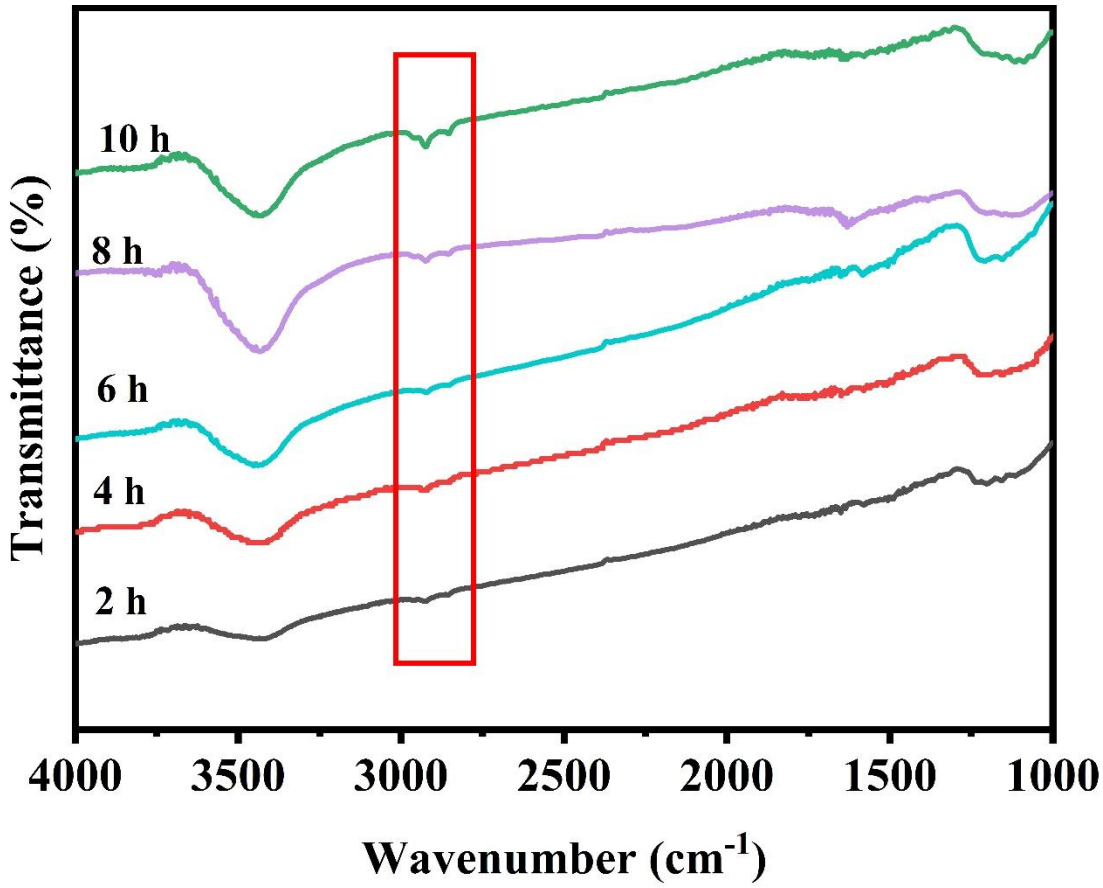

Figure S14 FT-IR spectra of PG electrodes after different reaction time.

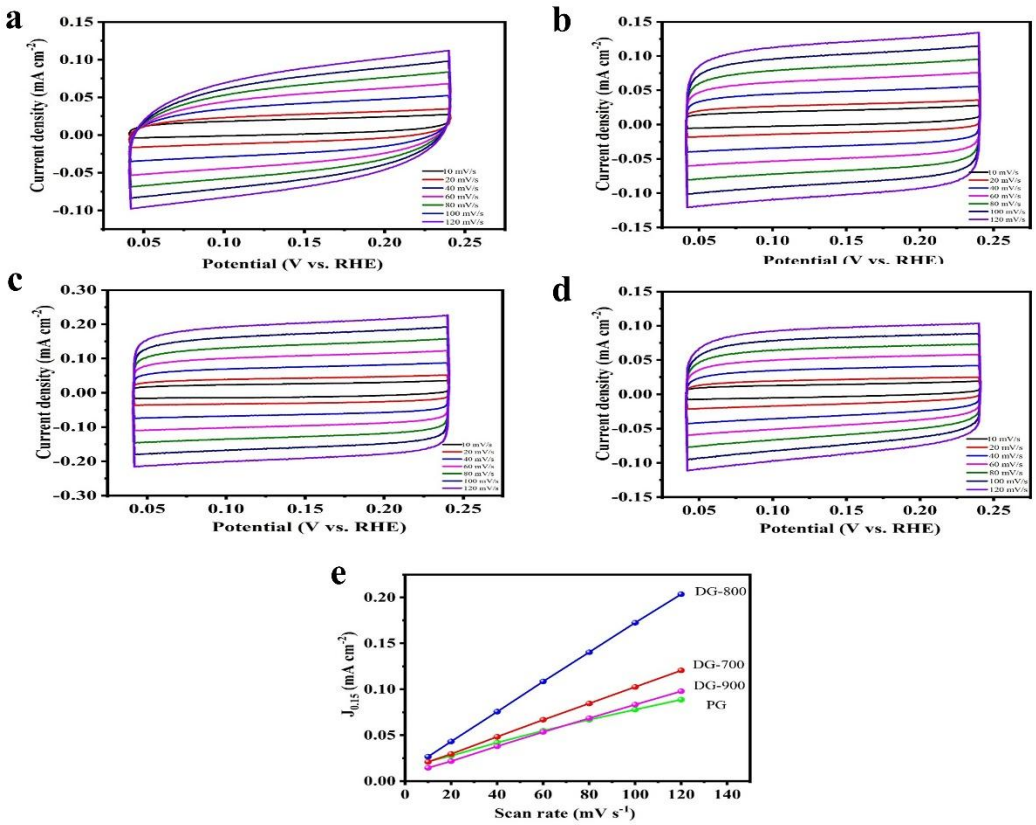

Figure S15 Cyclic voltammetry for the (a) PG; (b) DG-700; (c) DG-800; (d) DG-900; (e) charging current density at 0.15 V vs. RHE plotted against scan rates.

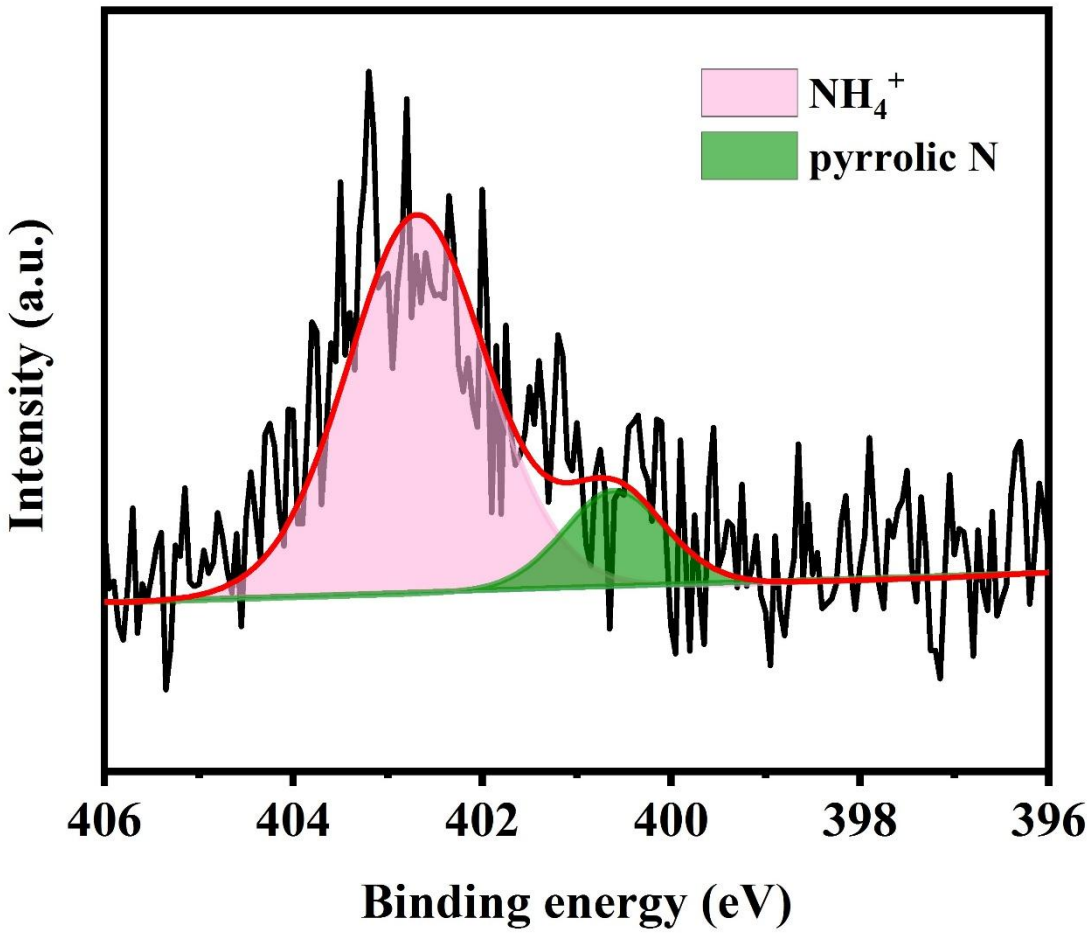

Figure S16 High-resolution N 1s XPS spectra of PG electrode after NRR at -0.4 V vs. RHE in N_2-saturated 0.01 M H_2SO_4 for 6 h.

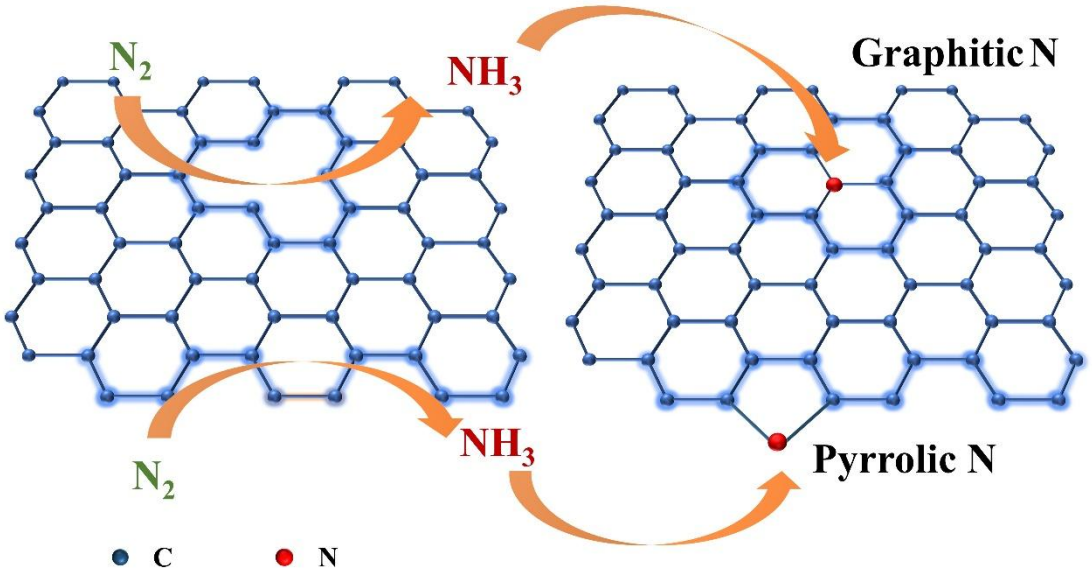

Figure S17 Schematic illustration of the NRR process and following N doping process on point defect and edges of defect graphene.

We speculated that pyrrolic nitrogen tends to originate from armchair edges, as it may be easy for chemically active C atoms on armchair edges to accept N to form a pentagon heterocyclic ring. Similarly, one possible configuration to form graphitic N is point defect, where the point is substituted by a N atom.

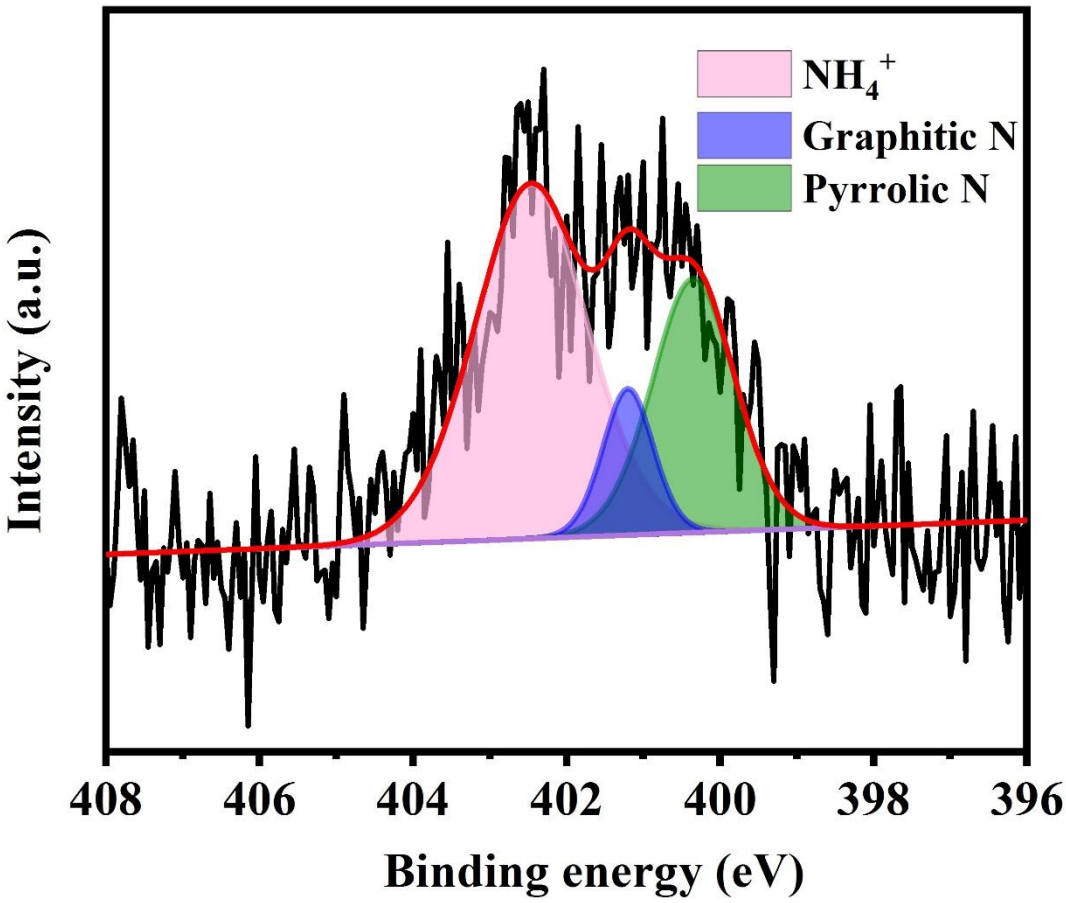

Figure S18 High-resolution N 1s XPS spectra of DG-800 electrode after NRR at -0.4 V vs. RHE in Ar-saturated $(NH_4)_2SO_4$ for 6 h.

III. Supplementary Tables

Table S1 Porosity properties of DG-800 and PG determined by N_2 adsorption-desorption measurements

Sample	S_{BET} (m^2 g^{-1}) [a]	V_{Tot} (cm^3g^{-1}) [b]	D_{Av} (nm)[c]
DG-800	420.20	0.58	5.82
PG	78.33	0.16	8.38

[a]: Surface area calculated based on Brunauer-Emmett-Teller (BET) method.

[b]: Total pore volume of pores at P/Po = 0.99

[c]: Barrett-Joyner-Halenda (BJH) Adsorption average pore width (4V/A)

Table S2 The comparable results of target product (NH_4^+) calculated based on Nessler and indophenol blue method.

	m(NH_4^+) determined by indophenol blue method (μg)	m(NH_4^+) determined by Nessler reagent (μg)	Absolute errors (μg)	Relative errors	Standard deviation
1	15.36	14.65	0.71	4.6%	0.5%
2	15.67	15.39	0.28	1.7%	0.2%
3	22.12	20.57	1.55	6.9%	1.1%

Table S3 XPS date of elemental compositions of DG-800 electrode surface before and after NRR

Atomic(%)	F	S	C	O	N
Before NRR	49.72	2.16	39.18	8.94	0
After NRR	47.98	1.85	40.50	8.27	1.40

Table S4 Nitrogen species in electrodes with catalyst after NRR obtained by fitting N 1s XPS spectra, the atomic ratios (%) and area ratio are listed in below table

Sample	Time	Electrolyte	NH_4^+	Graphitic nitrogen	Pyrrolic nitrogen	Area ratio[a]
DG-800	2 h	N_2-saturated H_2SO_4	69.26	30.74	0	1/0.22
DG-800	6 h	N_2-saturated H_2SO_4	68.99	16.20	14.81	1/0.18/0.07
DG-800	10 h	N_2-saturated H_2SO_4	51.55	13.72	34.73	1/0.27/0.67
DG-800	14 h	N_2-saturated H_2SO_4	47.38	9.64	42.98	1/0.20/0.91
PG	6 h	N_2-saturated H_2SO_4	83.75	0	16.25	1/0.19
DG-800	6 h	Ar-saturated $(NH_4)_2SO_4$	58.63	10.83	30.54	1/0.18/0.52

[a]: Area ratio was calculated by the area of three peaks: NH_4^+ (402.5eV), graphitic nitrogen (401.2 eV), pyrrolic nitrogen (400.1eV), where the area of NH_4^+ was normalized as 1.

Table S5 Ammonia yield and corresponding Faradaic efficiency of PG and DG-800

Sample	Potential	Absorbance	Concentration μg mL^{-1}	m (NH_4^+) μg	Rate μg $h^{-1}m_{cat}^{-1}$	Qc	FE%
PG	-0.3 V	0.055	0.0136	1.088	0.272	0.58	2.99
	-0.4 V	0.074	0.0516	4.128	1.032	1.58	4.19
	-0.5 V	0.09	0.0836	6.688	1.672	2.99	3.59
	-0.6 V	0.086	0.0756	6.048	1.512	4.42	2.20
DG-800	-0.3 V	0.087	0.0776	6.208	1.552	1.46	6.82
	-0.4 V	0.156	0.2156	17.248	4.312	3.26	8.51
	-0.5 V	0.115	0.1336	10.688	2.672	4.19	4.10
	-0.6 V	0.121	0.1456	11.648	2.912	5.30	3.54

References:

[1] Y. Zhao, R. Shi, X. Bian, C. Zhou, Y. Zhao, S. Zhang, F. Wu, G. I. N. Waterhouse, L. Z. Wu, C. H. Tung, T. Zhang, *Advanced Science* **2019**, *6*, 1802109.

[2] A. D. Smolenkov, I. A. Rodin, O. A. Shpigun, *J. Anal. Chem.* **2012**, *67*, 98-113.

[3] B. Delley, *The Journal of Chemical Physics* **2000**, *113*, 7756-7764.

[4] J. P. Perdew, K. Burke, M. Ernzerhof, *Phys. Rev. Lett.* **1996**, *77*, 3865-3868.

[5] B. Delley, *The Journal of Chemical Physics* **1990**, *92*, 508-517.

[6] M. Dolg, U. Wedig, H. Stoll, H. Preuss, *The Journal of Chemical Physics* **1987**, *86*, 866-872.

[7] A. Bergner, M. Dolg, W. Küchle, H. Stoll, H. Preuß, *Mol. Phys.* **1993**, *80*, 1431-1441.